Fractional solubility of iron in mineral dust aerosols over coastal Namibia: a link with marine biogenic emissions?

Karine Desboeufs[1], Paola Formenti[1], Raquel Torres-Sánchez[2,3], Kerstin Schepanski[4,$], Jean-Pierre Chaboureau[5], Hendrik Andersen[6,7], Jan Cermak[6,7], Stefanie Feuerstein[4], Benoit Laurent[1], Danitza Klopper[8,*], Andreas Namwoonde[9], Mathieu Cazaunau[2], Servanne Chevaillier[2], Anaïs Feron[1,%], Cécile Mirande-Bret[1], Sylvain Triquet[1], and Stuart J. Piketh[8]

[1] Université Paris Cité and Université Paris Est Créteil, CNRS, LISA, F-75013 Paris, France
[2] Université Paris Est Créteil and Université Paris Cité, CNRS, LISA, F-94010 Créteil, France
[3] CIQSO, Robert H. Grubbs Building, University of Huelva, Campus El Carmen, E21071 Huelva, Spain
[4] TROPOS, Leipzig, Germany
[5] Laboratoire d'Aérologie (LAERO), Université de Toulouse, CNRS, UT3, IRD Toulouse, France
[6] Institute of Meteorology and Climate Research, Karlsruhe Institute of Technology (KIT), Karlsruhe, Germany
[7] Institute of Photogrammetry and Remote Sensing, Karlsruhe Institute of Technology (KIT), Karlsruhe, Germany
[8] North-West University, School for Geo- and Spatial Sciences, Potchefstroom, South Africa
[9] SANUMARC, University of Namibia, Henties Bay, Namibia

* Now at University of Limpopo, Department of Geography and Environmental Studies, Sovenga, South Africa
[$] Now Institute of Meteorology, Freie Universität Berlin, Berlin, Germany
[%] Now at Université Paris-Saclay, INRAE, AgroParisTech, UMR ECOSYS, Palaiseau, France

Corresponding author: paola.formenti@lisa.ipsl.fr

Abstract

This paper presents the first investigation of the solubility of iron in mineral dust aerosols collected at the Henties Bay Aerosol Observatory (HBAO), in Namibia, from April to December 2017. During the study period, 10 intense dust events occurred. Elemental iron reached peak concentrations as high as 1.5 µg m^{-3}, significantly higher than background levels. These events are attributed to wind erosion of natural soils from the surrounding gravel plains of the Namib desert. The composition of the sampled dust is found to be overall similar to that of aerosols from northern Africa, but characterised by persistent and high concentrations of fluorine, which are attributed to local fugitive dust.

The fractional solubility of Fe (%SFe) for both the identified dust episodes and background conditions ranged between 1.3 to 20 % and averaged at 7.9% (± 4.1%) and 6.8 (± 3.3%), respectively. Even in background conditions, the %SFe was correlated to that of Al andSi. The solubility was lower between June and August, and increased from September onwards, during the austral spring. The relation with measured concentrations of particulate MSA (methane sulfonic acid), solar irradiance and wind speed suggests a possible two-way interaction whereby marine biogenic emissions from the coastal Benguela upwelling to the atmosphere would increase the solubility of iron-bearing dust, according to the photo-reduction processes. This first investigation points to the west coast of southern Africa as a complex environment with multiple processes and active exchanges between the atmosphere and the Atlantic Ocean, requiring further research.

Keywords: aerosols, mineral dust, water-soluble Fe, atmospheric processing, marine biogenic emissions

1. Introduction

Through the processes of atmospheric transport and deposition, mineral dust is known to provide nutrients and metals to the terrestrial and marine ecosystems (Hooper et al., 2019; Ventura et al., 2021). Amongst those, mineral dust provides iron (Jickells et al., 2005), which plays a major role for the primary productivity of the nutrient-limited oceans, modulating the marine carbon cycle (Hooper et al., 2019) as well as that of key continental ecosystems such as the Amazon rainforest (Reichholf, 1986).

To date, much attention has been paid to the soluble Fe in mineral dust emitted from arid and semi-arid areas in the northern Hemisphere, in particular the Saharan and Chinese deserts (e.g. Baker et al., 2006; Paris et al., 2010; Takahashi et al., 2011; Rodriguez et al., 2021), where emissions are the most intense (Tegen and Schepanski, 2009). Nonetheless, the southern Hemisphere accounts for approximately 10% of the global atmospheric dust loading (Kok et al., 2017). Large sources are found in southern Africa, mostly in Namibia (Kalahari and Namib deserts, Etosha Pan, numerous ephemeral riverbeds along the Namibian coastline) and Botswana (Makgadikgadi Pan) (Prospero et al., 2002; Bryant et al., 2007; Mahowald et al., 2003; Ginoux et al., 2012; Vickery and Eckardt, 2013; Von Holdt et al., 2017).

Previous research has shown that the long-range transport of dust emitted from southern African sources can reach the south-eastern Atlantic and the Indian Oceans (Swap et al., 1996; Jickells et al., 2005; Bhattachan et al., 2012; 2015; Ito and Kok, 2017). In particular, Gili et al. (2022) demonstrated recently that mineral dust from Namibia can also be transported across the Southern Ocean to eastern Antarctica. Furthermore, the research by Dansie et al. (2022) has suggested that mineral dust from Namibia could dominate the atmospheric deposition to the coastal Benguela Upwelling System (BUS), where biomass burning aerosols, a significant source of soluble Fe to the Southern and Indian Oceans (Hamilton et al., 2021; Ito et al., 2021; Liu, et al., 2022), are limited by atmospheric stratification (Formenti et al., 2019; Redemann et al., 2021). The inputs of Namibian (and Angola) dust in the upwelled waters could also modulate the migration of skipjack tuna between the Gulf of Guinea and the equatorial Atlantic, by contributing to support phytoplankton growth and hence upper trophic levels in this area (Rodriguez et al., 2023).

There is, however, very little data available on the concentrations and composition of soluble Fe in dust aerosols from southern Africa, both near the sources and over the oceans. Previous research in Namibia focussed on soils and sediments (Dansie et al., 2017a; 2017b; Kangueehi, 2021). The Atlantic Meridional Transect (AMT) cruise programme conducted recurrent observations between October and March in the South Atlantic Ocean (Baker et al., 2013), while Heimburger et al. (2013) and Gao et al. (2013) report on sparse measurements of deposited aerosols and in rainwaters over the Southern Indian Ocean.

Within this context, this paper investigates the fractional solubility of Fe (%SFe) in samples of atmospheric aerosol particles smaller than 10 µm in diameter collected in 2017 at the Henties Bay Aerosols Observatory (HBAO) on the Namibian coast. In section 2 we outline the experimental and analytical methodology for elemental and water-soluble analysis of ions and metals, including iron. We also provide the definition of fractional solubility and the method for estimating the total dust mass. We introduce the supporting tools used to evaluate the source regions of the collected mineral dust, their pathways during transport, and the presence of fog, a recurrent feature on coastal Namibia favouring multi-phase ageing processes. Section 3 provides the results of the analysis. We present the iron soluble concentrations and solubility, and explore their links to the load, emission area and transport of mineral dust, as well as atmospheric processing. Section 4 discusses the observations, suggesting that the %SFe in the Namibian dust is higher when the MSA (methane sulfonic acid), a tracer of marine biogenic emissions, is also detected in these highest concentrations. This points to the photo-oxidation of DMS (Dimethyl Sulfide) as a process for increasing the Fe solubility, and suggests a possible positive feedback loop of the iron fertilisation by dust to the ocean. Section 5 summarizes the findings and suggests directions for future research.

2. Methodology

2.1. Study area

The HBAO (22.09°S, 14.26°E; http://www.hbao.cnrs.fr/, last access: 10 October 2022) is located at the Sam Nujoma Marine and Coastal Resources Research Centre (SANUMARC) of the University of Namibia in Henties Bay, Namibia (Fig. 1).

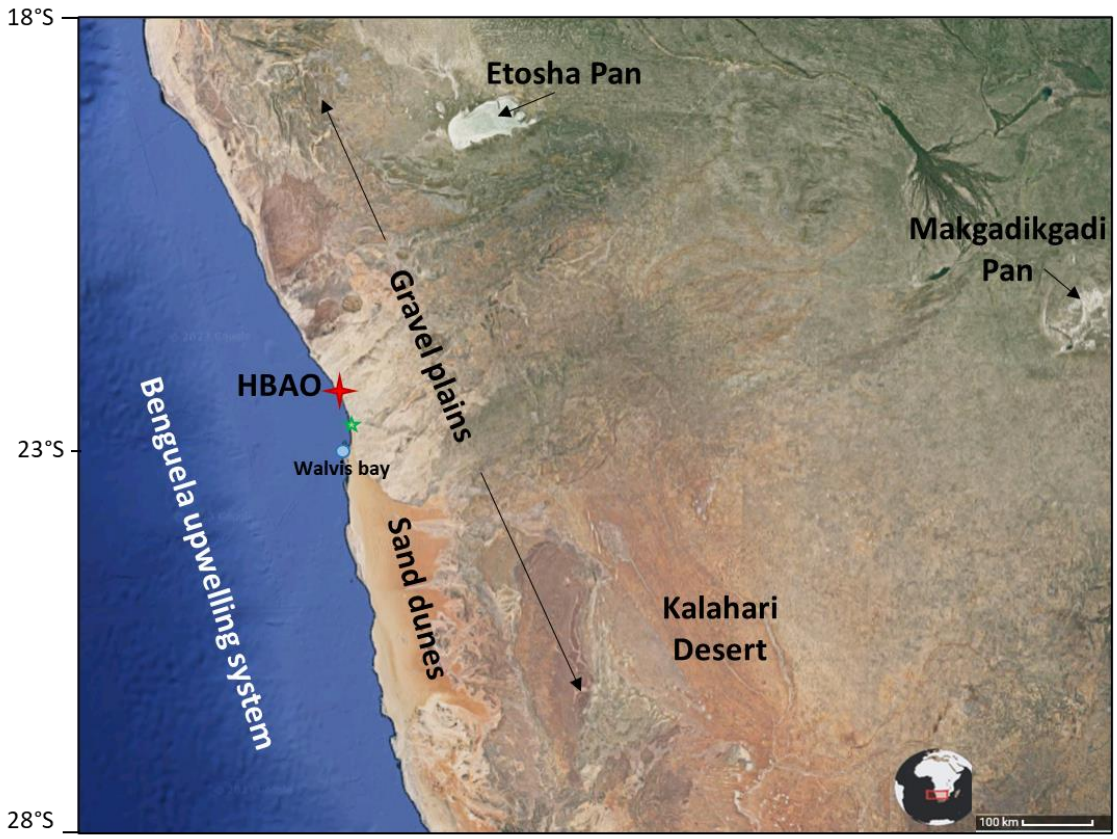

Figure 1: Location of Henties Bay Aerosol Observatory (HBAO, red star) and main dust source regions (© Google Maps). The position of Walvis Bay (blue dot), the major harbour in the area, and the Wlotzkasbaken meteorological station (green star) are also indicated.

Three kilometers to the south of the University campus hosting HBAO is the small town of Henties Bay, with no industrial activity and very little traffic, and approximately 170 km north from Walvis Bay, the major harbour in Namibia. Directly east of HBAO are the Namibian gravel plains, which are one of the dominant features of the Namib desert together with the sand dunes. Approximately 100 m to the north is the Omaruru riverbed, one of the coastal sources of mineral dust identified by Vickery and Eckardt (2013).

Our previous results show that, at the surface level, the atmosphere at HBAO is a receptor of different air masses dominated by marine aerosols, but also the seasonal occurrence of light-absorbing aerosols from biomass burning or pollution in northern wind regimes, and mineral dust detected episodically from various wind directions (Formenti et al., 2018; Klopper et al., 2020, hereafter KL20).

2.2. Sample collection and analysis

Aerosol particles smaller than 10 µm in aerodynamic diameter (PM_{10}) were collected by an automated sampler (model Partisol Plus 2025i, Thermo Fisher Scientific, Waltham, MA USA) on 47 mm Whatman Nuclepore polycarbonate filters (1-µm pore size). The air was drawn through a certified sampling inlet (Rupprecht and Patashnick, Albany, New York, USA) located at approximately 30 m above

ground and operated at a flow rate of 1 m^3 h^{-1}. Samples were collected for 9 hours during the daytime (from 9:00 to 18:00 UTC time) and night-time (21:00 to 06:00 UTC time) for 12 non-consecutive weeks from April to December 2017 (7-14 April, 26 April-3 May, 19-26 May, 07-14 July, 2-9 August, 15-22 August, 18-25 September, 02-09 October, 31 October-7 November, 13-20 November, 28 November-04 December, 12-19 December). In total, 176 samples (+ 13 blanks, one per week of sampling) were collected.

The elemental analysis of 24 elements from Na to Pb, including some major tracers of mineral dust (Fe, Al and Si), was performed at the LISA laboratory by Wavelength-dispersive X-ray fluorescence (WD-XRF) using a PW-2404 spectrometer (Panalytical, Almelo, Netherlands), as detailed by KL20. The total mass concentration per element x will be referred to as TX.

The measured elemental concentrations are used to calculate the estimated dust mass (*EDM*) according to Lide (1992) as

$$EDM = 1.12 \times \{1.658 \times [\text{nss-Mg}] + 1.889 \times [Al] + 2.139 \times [Si] + 1.399 \times [\text{nss-Ca}] + 1.668 \times [Ti] + 1.582 \times [Mn] + (0.5 \times 1.286 + 0.5 \times 1.429 + 0.47 \times 1.204) \times [Fe]\} \quad (1)$$

where, as explained by KL20, nss-Mg and nss-Ca represent the non-sea salt fractions of Mg and Ca, respectively.

The analysis of the water-soluble fraction was also performed at LISA. Individual filters were placed in 20 mL of ultrapure water (MilliQ® *18.2* MΩ.cm) for 30 minutes. The solution was filtered (Nuclepore polycarbonate filters with 0.2µm pore size) then divided into two sub-samples. One half was analysed by Ion Chromatography (IC) using a Metrohm IC 850 device equipped with a column MetrosepA supp 7 (250/4.0 mm) for anions and with a Metrosep C4 (250/4.0 mm) for cations. The IC analysis provided the concentrations of the following water-soluble ions: F^-, Cl^-, NO_3^-, SO_4^{2-}, formate, acetate, oxalate, MSA^- (methanesulfonic acid), Na^+, NH_4^+, K^+, Ca^{2+} and Mg^{2+}. A calibration with certified standard multi-ions solutions of concentrations ranging from 5 to 5000 ppb was performed and the uncertainty of the analysis was estimated to be 5% (KL20).

The second half of the solution was acidified to 1% with ultrapure nitric acid (HNO_3) and analysed by Inductively Coupled Plasma-Atomic Emission Spectroscopy (ICP-AES) using a Spectro ARCOS Ametek® ICP-AES and by High-resolution Inductively Coupled Plasma-Mass Spectrometry (HR-ICP-MS) using a Neptune Plus™ instrument by Thermo Scientific™. The calibration curve was performed using standard multi-element solutions ranging from 2 to 1000 ppb for ICP-AES and 1 to 1000 ppt for HR-ICP-MS (Desboeufs et al., 2022). These analyses provided the dissolved mass concentrations (DX) of 25 water-soluble metals and metalloids, including Fe, Al, and Si. All sample concentrations were corrected using the filter blanks for each sampling period.

Based on those analyses, the fractional solubility (%SX) representing the percentage solubility value was calculated as

$$\%SX = 100 \times DX/TX \quad (2)$$

with DX and TX, the dissolved and total elemental concentration respectively.

Here, a leaching protocol using ultrapure water (UPW) was used to simulate wet deposition of particles, since the wet deposition dominates the total iron supply in the Southern Atlantic Ocean (Chance et al., 2015). Moreover, the UPW leach enables the chemical reaction between iron with organic or inorganic ligands, naturally dissolved from the particulate aerosols into rain droplets. However, it is known that the extraction protocol modulates dissolution process and hence the values of %SFe, in particular the estimates using UPW are higher in comparison to these one using seawater, but lower than the acidic, buffered or reduction agent leach (Perron et al., 2020).

2.3. Ancillary data

Maps of the emission fluxes of mineral dust were calculated using the dust emission model described by Feuerstein and Schepanski (2019), driven with hourly 10m wind fields at a 0.1° x 0.1° grid from the European Centre for Medium-range Weather Forecasts (ECMWF). The dust emission parameterisation follows Marticorena and Bergametti (1995). Additional information on the soil type was taken from the ISRC soil data set (FAO/IIASA/ISRIC/ISSCAS/JRC, 2012) and information on the aerodynamic roughness length was obtained from POLDER/ADEOS surface products following the works of Marticorena et al. (2004) and Laurent et al. (2005). The MODIS monthly vegetation product (MYD13A3 v6) was used to describe the vegetation cover, while the vegetation type was defined using the BIOME4 database (Kaplan et al., 2003). We additionally differentiated between different dust source types (alluvial fines, dunes and sand sheets) which allowed us to reflect the source diversity over Namibia and thus the spatial diversity in the soil's susceptibility to wind erosion. This layer was compiled following Feuerstein and Schepanski (2019) using MODIS surface reflectance (MOD09A1 v6). A MODIS retrieved map on surface water cover was used to eliminate flooded areas as active dust sources.

Back-trajectories of the air masses during the dust events were calculated from Meso-NH model (version 5.3). The model set-up is similar to the one used for the AErosols, RadiatiOn and CLOuds in southern Africa (AEROCLO-sA) field campaign (Formenti et al. 2019) and related case studies (Flamant et al. 2022; Chaboureau et al. 2022). In short, the model was run on a 5 km grid covering the southern tip of Africa and 67 stretched levels spaced by 60 m close to the surface and 600 m at high altitude. Meso-NH was run for 24 h for each dust event using initial and boundary conditions provided

by the ECMWF operational analysis. Emission, transport and deposition of dust is described by the scheme of Grini et al. (2006). Back trajectories were computed online using three passive tracers initialized with the 3D-field of their initial conditions. Further details on the dust prognostic scheme, the backward trajectories and the physical parameterizations are given in Chaboureau et al. (2022).

The presence of fog and low clouds (FLC) along the Namibian coastline during dust events was analysed using an existing satellite-based fog and low-cloud data set (Andersen et al., 2019). The FLC detection algorithm used to create this data set was developed and validated specifically for this region. The algorithm is based on infrared observations from the Spinning Enhanced Visible and Infrared Imager (SEVIRI) aboard the geostationary Meteosat Second Generation (MSG) satellites, making use of both spectral and textural information. The FLC product is available at the native spatial and temporal resolutions of the SEVIRI sensor (3 km nadir, every 15 minutes), as described in Andersen and Cermak (2018). The FLC product does not specifically distinguish between fog and low clouds but captures the coastal boundary-layer cloud regime typical for the region and at HBAO that could interact with mineral dust. It has been shown to be consistent with synoptic-scale atmospheric dynamics (Andersen et al. 2020). The FLC data are used to calculate maps of average fog and low cloud coverage for the time periods of all dust events given in Table 1.

Observations of the local meteorology, including measurements of air temperature, relative humidity and fog, at the nearby Wlotzkasbaken meteorological station (22.31°S, 14.45°E, 73 m asl, see Fig. 1) part of the Southern African Science Service Centre for Climate Change and Adaptive Land Management (SASSCAL) ObservationNet (https://www.sasscal.org/; last accessed 14/04/2023), are used.

3. Results

3.1. Description of the dust episodes

The dataset discussed in this paper is based on 176 aerosol samples collected at HBAO, 42 of which were associated with 10 dust episodes. As detailed by KL20, events of mineral dust were identified as peaks in the time series of the mass concentrations of Al and non-sea-salt Ca^{2+} (nss-Ca^{2+}). The dust episodes investigated in this study are a subset of those presented by KL20, we therefore use their naming convention to facilitate the connections between the two papers (Table 1). In the following, we refer to samples collected during the dust episodes as “dust”. Samples collected outside the dust events will be indicated as “background”.

Table 1. Dates of dust events identified at HBAO from May to December 2017, following KL20. The number of samples collected during each episode is indicated in the column called “N”. The average air temperature, relative humidity, wind speed and direction recorded at the nearby meteorological station in Wlotzkasbaken are reported. The maxima wind speed and corresponding direction are indicated in brackets in the corresponding columns. The average EDM is reported with in brackets the maximum of EDM during the event.

Episode identifier	Start and end date (UTC)	N	Air temperature (°C)	RH (%)	Wind speed ($m\ s^{-1}$)	Wind direction (degN)	EDM ($\mu g\ m^{-3}$)
Dust 04	19/05 09h – 20/05 18h	3	17.7	73.7	2.7 (6.2)	186 (185)	13 (14)
Dust 05	24/05 21h – 26/05 09h	3	18.1	63.3	2.3 (6.3)	183 (188)	21 (42)
Dust 06	11/07 09h – 13/07 09h	4	13.2	82.9	1.2 (5.4)	235 (193)	27 (45)
Dust 07	04/08 21h – 06/08 09h	4	12.5	87.0	1.2 (5.4)	233 (201)	10 (16)
Dust 08	17/08 21h – 19/08 09 h	4	11.9	80.6	1.3 (4.6)	324(129)	18 (21)
Dust 09	23/09 21h – 24/09 18h	2	15.6	84.3	3.1 (6.2)	309 (330)	11 (17)
Dust 10	05/10 21h – 08/10 09h	8	14.0	74.6	2.1 (5.9)	249 (228)	14 (23)
Dust 11	15/11 09h – 18/11 09h	6	16.7	66.1	3.2 (11.7)	231 (232)	31 (56)
Dust 12	30/11 09h – 01/12 18h	3	16.7	78.1	1.9 (5.7)	244 (195)	2 (3)
Dust 13	15/12 09h – 19/12 09h	7	16.9	76.9	2.9 (6.5)	252 (238)	10 (19)

The dust episodes were long-lasting (generally a few days). The dynamic of the emissive areas, air mass transport and fog coverage during the episodes (Fig. 2 and S1) is driven by the synoptic circulation, which, in southern Africa, is primarily affected by the high-pressure belt under the descending limb of the Hadley cell (Tyson and Preston-Whyte, 2014). The maps of dust emission fluxes and the air mass back-trajectories reflect this seasonality. During the first part of the year (episodes Dust 04 to 05), dust emissions originated from the gravel plains and the Etosha pan north of HBAO. During this time of the year the transport to HBAO below 300 m asl was north- to south-easterly originating inland from the coast.

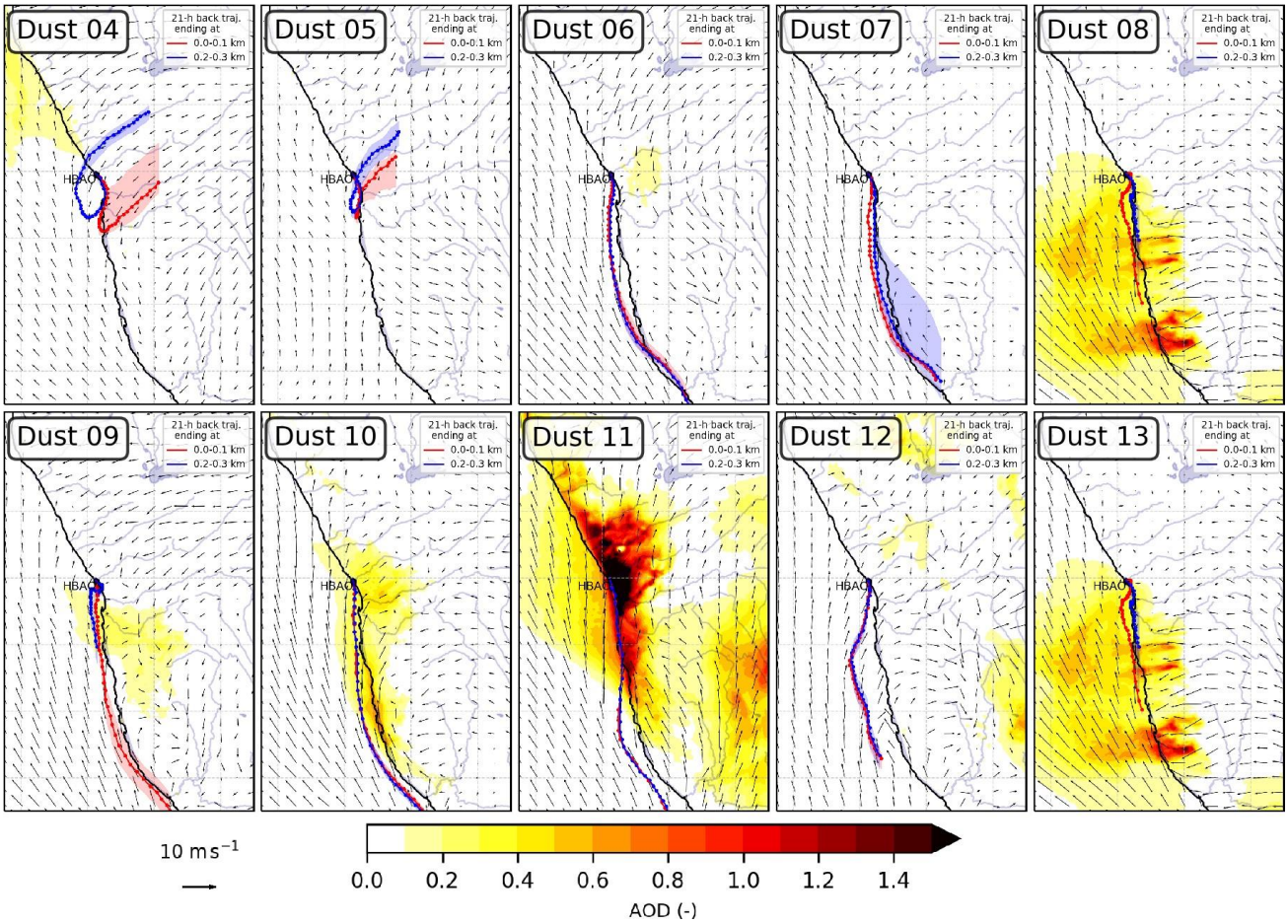

Figure 2: Maps of dust optical depth (shading) and 10-m wind (vector) overlaid by pathway of 21-hour air mass back trajectories ending in the first 100 m (red line) and between 200 and 300 m (blue line) above HBAO for dust episodes, as calculated by the Meso-NH model (version 5.3). Dots are plotted every hour and shadings around these lines are the interquartile ranges for latitudes.

From July onwards, the active source areas were identified in the southern gravel plains, Namib sand dunes and Kalahari Desert (this former source only for Dust 11 to 13). Air mass transport was southerly and travelled over the sea and along the coastline. It is worth noticing that all the air masses experienced maritime air during their last hours of transport, including the episodes Dust 04 and 05 associated with berg wind conditions, due to the coastal low that develops to the west of HBAO.

The formation of fog events at Henties Bay is also highly seasonal. The frequency of occurrence of fog events is highest during austral winter at the coast, whereas lifted stratus clouds dominate during austral summer, when overall FLC occurrence peaks. The occurrence of fog over Namibia correspond to the advection of low-level clouds which is modulated both by local meteorology along the coastline of Namibia (trade winds) and synoptic-scale radiative processes (Spirig et al., 2019; Andersen et al., 2019; 2020). Henceforth, as shown in Fig. S1, the presence of fog and low clouds correlates with wind directions and aerosol source regions. Overall, three episodes (Dust 04, Dust 05 and Dust 11 in April, May and November, respectively) occurred in fog-free or low-fog conditions. The remaining episodes were characterised by extensive fog and low cloud coverage throughout the study area. The

meteorological observations at the nearby Wlotzkasbaken station (Fig. S2) confirm these findings, and show in particular that the relative humidity always exceeded 60 %, and 80 % when fog or low clouds were present (Table 1). As a consequence, the aerosol can be considered deliquescent even in the fog-free conditions. The seasonality is also observed in the average downwelling solar irradiance, with the lowest values during July and September, associated with austral winter. Finally, it is interesting to note that the fog-free conditions, associated with the predominance of continental air masses, corresponded to the highest EDM, possibly because of the reduced wet removal during transport and the increase of emission fluxes with the decrease of soil moisture (Kok et al., 2014), but possibly also because of the high wind speed prevailing during these conditions, which in principle, enhances both dust emissions and transport (Table 1).

3.2. Iron solubility

The total and dissolved concentrations, and fractional solubility of Fe, Al and Si, during the dust episodes are reported in Table 2**,** where they are compared to background conditions. For iron, the average values over the entire sampling period are also shown.

Table 2. Average and standard deviations of water-soluble (DX), total elemental (TX) mass concentrations and fractional solubility (%SX) for Fe, Al and Si at HBAO measured for the total period and during the dust and background events from April to December 2017. Concentrations values are expressed in ng m^{-3}, while fractional solubility is expressed in percent. The numbers of considered samples is presented between the parentheses.

	Fe			**Al**		**Si**	
	All period	**Dust**	**Background**	**Dust**	**Background**	**Dust**	**Background**
DX	28 ± 51 *(N=175)*	80 ± 84 *(N=42)*	11 ± 10 *(N=131)*	322 ± 296 *(N=42)*	56 ± 46 *(N=131)*	529 ± 616 *(N=42)*	78 ± 83 *(N=124)*
TX	364 ± 482 *(N=176)*	955 ± 633 *(N=42)*	177 ± 155 *(N=133)*	1204 ± 870 *(N=42)*	284 ± 222 *(N=94)*	4158 ± 3037 *(N=42)*	776 ± 674 *(N=133)*
%SX	7.1 ± 3.6 *(N=175)*	7.9 ± 4.1 *(N=42)*	6.8 ± 3.3 *(N=130)*	27 ± 10 *(N=42)*	26 ± 11 *(N=90)*	12 ± 7 *(N=42)*	11 ± 8 *(N=116)*

The total Fe concentrations varied significantly from one episode to the other, and so did EDM, which was larger than 10 µg m^{-3} for all of them (except Dust 12) and as high as 56 µg m^{-3} during Dust 11 event (Table 1). By contrast, the total Fe-to-EDM ratio was virtually constant, with an average of 5.8 % (± 0.6 %) for the dust events and 5.6 % (± 1.1%) for the entire dataset. These values are quite superior to usual Fe content recommended in upper continental crust models (3.5% for Taylor and McLennan or 5.04 +/- 0.53 % Rudnick and gao, 2004) and estimated in Saharan dust (4.45% for Guieu et al., 2002; 4.3 to 6.1% for Lafon et al., 2006 or 4.5% for Formenti et al., 2008). Keeping in mind that Fe abundance is estimated, this suggests that the Namibian aerosol dust could be enriched in iron in comparison to upper crust and dust provided by Saharan sources.

The total dissolved concentrations of Fe during the sampling period ranged from 1.5 to 427 ng m^{-3}, with a median and average of 10.5 and 28 ng m^{-3}. During the dust episodes, the average mass concentration of dissolved Fe was 80 ± 84 ng m^{-3}, almost an order of magnitude higher than for background conditions (11 ± 10 ng m^{-3}). The dissolved concentrations in dust periods are higher than those observed in the South Atlantic Ocean for air masses associated with transport from continental southern Africa (Baker et al., 2013; Chance et al., 2015; Baker and Jickells, 2017), which are of the order as those observed at HBAO for background periods. The calculated %SFe ranged from 1.3 to 19.8 %, with a median and average of 6.7 and 7.1 %. The average %SFe during dust events (7.9 ± 4.1%) was higher, but quite similar than in background conditions (6.8 ± 3.3%). It is interesting to note that Dust 11 event, the most intense recorded event, presents the highest %SFe (between 10.2 and 19.8 % with an average at 13.8 %). Apart from this event, the average fractional solubility seems to be independent of the EDM. Excluding this event, the average solubility of Fe for dust events (6.9 % ± 3.3 %) is equivalent to the one for background samples. The uniformity of %SFe values between background and dust periods contrasted with the observations made in regions where the dust influence is sporadic and the origin of Fe is associated to various sources (e.g. Shelley et al., 2018). That is consistent with a main dust source of iron in our samples, as indicated in KL20. For both conditions, the observed range of variability is high and consistent with previous observations over the Southern Atlantic Ocean (2.4-20 %, Baker et al., 2013; 1.3-22 %, Chance et al., 2015), and the Southern Indian Ocean (0.76-27 %, Gao et al., 2013), using acetate buffer leach at pH 4.7 (0.4µm) which can extract 1.4 times more Fe than UPW protocol (Perron et al., 2020). Moreover, the measured %SFe is significantly higher than obtained from dissolution experiments, with an identical protocol, of mineral dust aerosol samples collected on filters after laboratory generation from the soils collected in Namibian sources (< 1%; Formenti et al., in preparation, 2024).

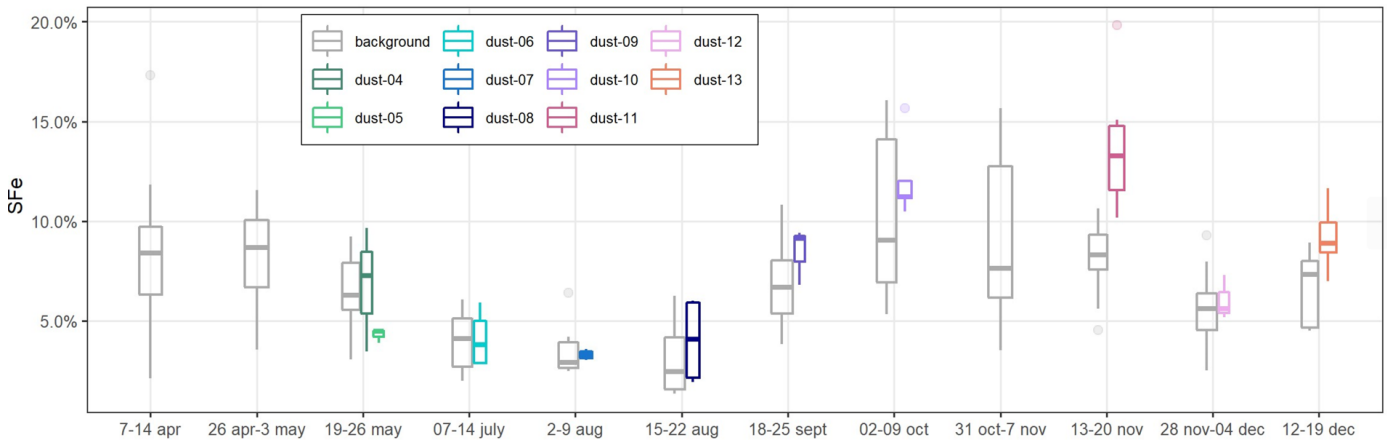

Figure3: Temporal variability of %SFe average for dust and background samples during the different periods of sampling. In the box plots, the box indicates the interquartile range, i.e. the 25th and the 75th percentile, and the line within the box marks the median. The whiskers indicate the quartiles ±1.5 times

the interquartile range. Points above and below the whiskers indicate outliers outside the 10th and 90th percentile.

The temporal variability of %SFe is presented in Fig. 3, where dust and background episodes are shown separately. The temporal variability is similar during dust and background conditions. The highest %SFe occurred during austral spring (October-November), and in particular during episode Dust 11 from 13 to 20 November 2017, when the average %SFe reached 13.8 %. The %SFe was quite similar along the year between dust and background, except between 13-20 November where the iron solubilities during Dust 11 event was very superior to the one of background samples, and to a lesser extent, in September (Dust 09) and December (Dust 13).

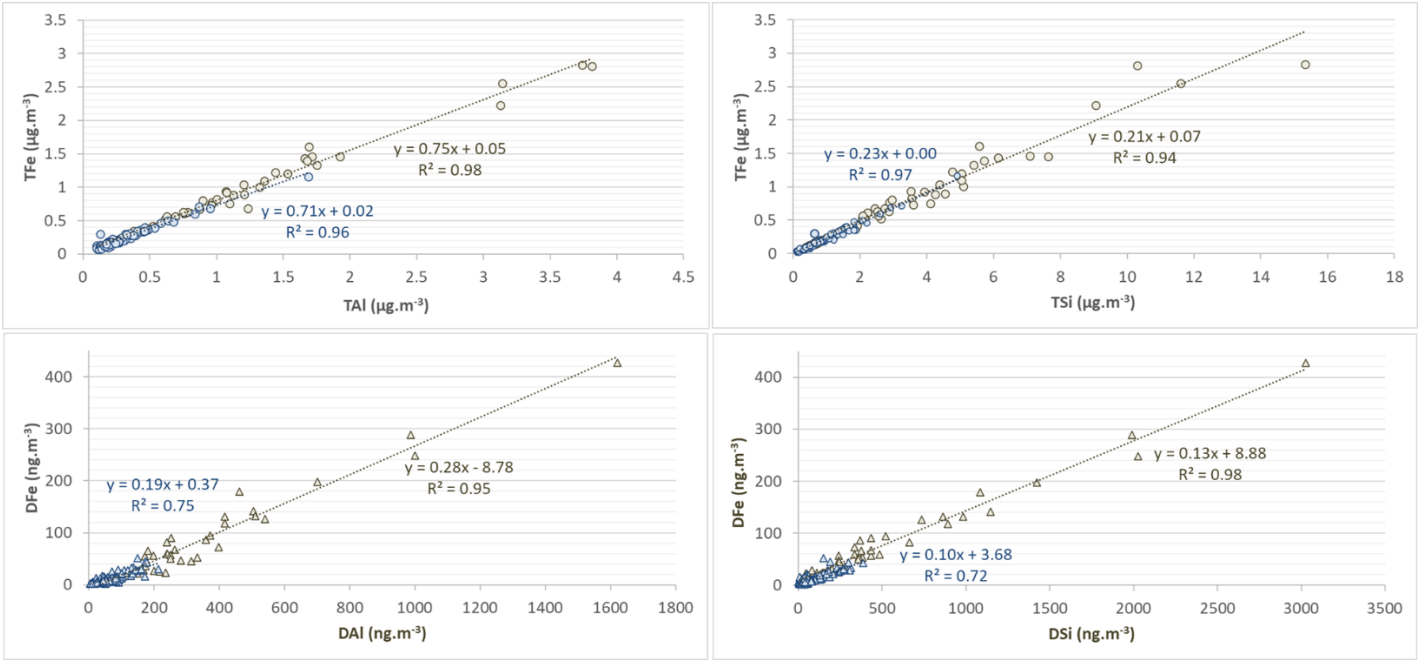

Figure 4: Scatterplot of TFe with respect to TAl and TSi (top panels) and DFe with respect to DAl and DSi (bottom panels) for dust (sand dots and triangles) and background events (blue dots and triangles). The Pearson coefficient are shown for both.

Figure 4 represents the correlations of Fe with Al and Si, both for the total and the dissolved concentrations. For both dust and background samples, the total Fe concentration is linearly correlated with total Al (R^2=0.98 and 0.96, slope=0.75 and 0.71, for dust and background conditions respectively) and total Si (R^2=0.94 and 0.97, slope=0.21 and 0.23, respectively). The slopes are consistent with typical Fe/Al and Fe/Si ratios found in desert dust from northern Africa (Formenti et al., 2011; Shelley et al., 2014), confirming the main crustal origin of Fe during all the sampling periods. Likewise, the concentrations of dissolved iron (DFe) show a strong linear correlation with both DAl and DSi, for both for dust and background events (R^2=0.96 and 0.75 with respect to DAl and R^2=0.98 and 0.73 with

respect to DSi). The slopes for Al and Si are also comparable (0.19 and 0.28 for DAl and 0.10 and 0.13 for DSi, respectively in dust and in background events). A very strong linear correlation was also observed between DFe and DTi (R^2=0.96 and 0.84; not shown), another unique marker of mineral dust. Significant correlations of soluble concentrations for several elements associated with mineral dust (Fe, Al, Si, Ti) have been previously obtained in remote aerosols over oceanic areas (Baker et al., 2016). Additionally, DFe during dust events correlate very closely with F^- (R^2=0.94, not shown), which has been indicated by KL20 as being emitted in the atmosphere by the wind erosion as well as the labouring of the Namibia soil, rich in fluoride mineral deposits.

4. Discussion

Several studies have shown that variations in aerosol Fe solubility could result from the source/composition of the aerosols. As a matter of fact, the Fe solubility has been linked to the iron mineralogy (Journet et al., 2008) and has been shown being lower for African crustal sources than in continental/anthropogenic sources (Desboeufs et al., 2005; Sholkovitz et al., 2009; Shelley et al., 2018). The iron fractional solubility in mineral dust is also affected by source mixing (Paris et al., 2010; Desboeufs et al., 2005), by (photo)chemical processing with acids or organic ligands during atmospheric transport (Paris et al., 2011, Paris et Desboeufs, 2013; Wozniak et al., 2013; Swan and Ivey, 2021) and by the increase of surface area to volume ratio due to size changes during transport (Baker & Jickells, 2006; Marcotte et al., 2020).

In the following sections, we discuss these possible factors to explain the seasonality and the extended range of variability of the %SFe in HBAO samples. The possible increase of surface area to volume ratio during transport (Baker and Jickells, 2006; Marcotte et al., 2020) will not be discussed because of lack of appropriate observations of the size distribution. Because of the similar transport time suggested by back trajectories (Fig. 2), it is likely that particle size distribution would be similar from one event to the other.

4.1. Influence of dust composition

Close to the dust source, iron solubility could be mainly conditioned by the mineralogical composition of dust (Journet et al., 2008, Formenti et al., 2014). Considering that soluble Fe-bearing aerosols were issued from mineral dust for all the samples, the seasonality of dust emission sources (see 3.1) could be a factor explaining the seasonality of %SFe (and other elements associated to mineral dust). Figure 5 shows the scatter plot of the elemental mass ratio of Fe/nss-Ca^{2+} and Si/Al, previously used for northern Africa dust to distinguish aerosol dust from source areas enriched in clays or iron oxides to soils rich in quartz or carbonates (Formenti et al., 2014). Specific to Namibia, because of the strong link between nss-Ca^{2+} and fluorine, the Fe/nss-Ca^{2+} ratio may also to distinguish dust influenced by fluorspar mining.

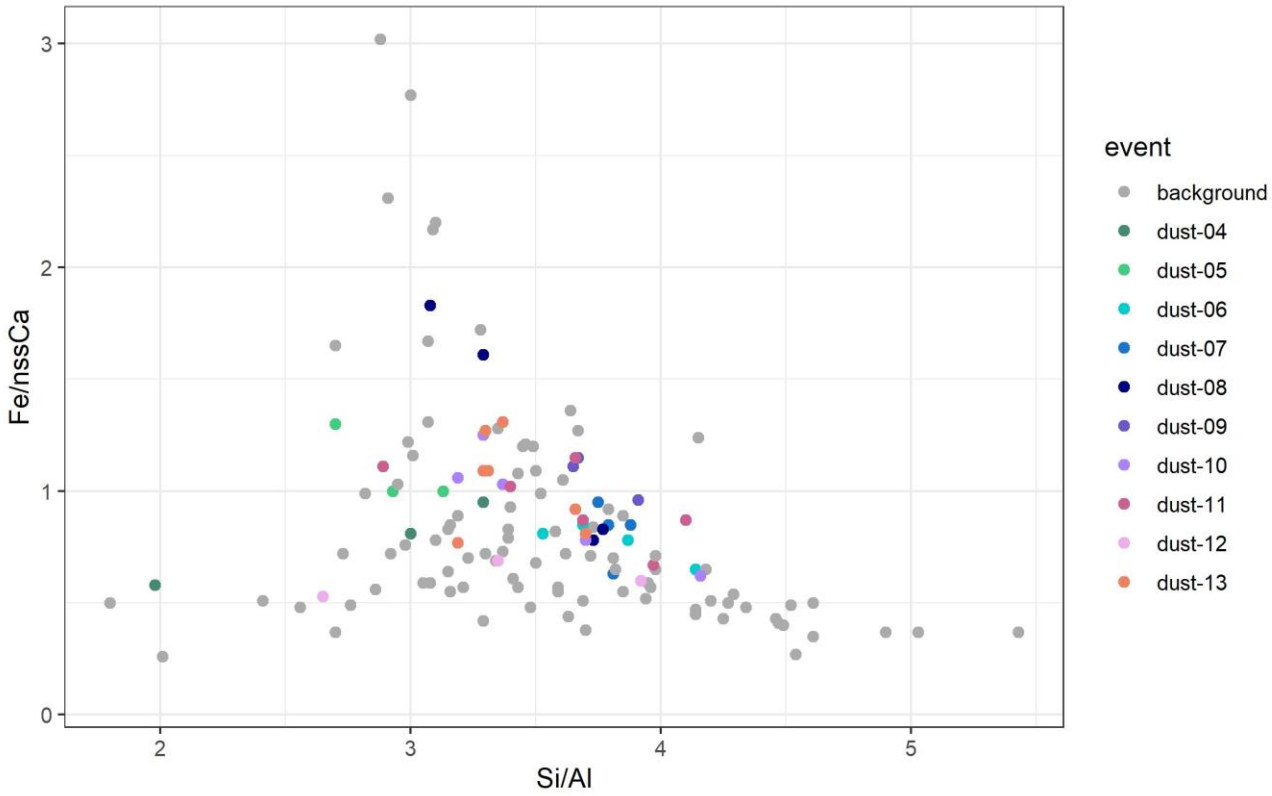

Figure 5: Scatterplot of Fe/nss-Ca^{2+} and Si/Al mass ratios for the samples collected at HBAO in period May-December 2017. Values obtained for samples collected during the dust events are represented as colored dots. Values for samples collected outside those events (background) are represented as grey dots.

Figure 5 indicates that the range of variability of both Fe/nss-Ca^{2+} and Si/Al ratios is small when considering dust events only. The elemental ratios of samples collected during the background periods are rather similar to dust events during a same sampling period, except for Si/Al for the period between 19-26 May and for Fe/nss-Ca^{2+} for the samples of 18-25 September, when significant differences, not really explicable and not inducing a significant difference in the %SFe values are observed (Fig. S3).

The values for ambient dust measured at HBAO are consistent with those of the previous field observations in Namibia (Annegarn et al., 1983; Eltayeb et al., 1993), but also with values reported by Caponi et al. (2017) for laboratory-aerosolised dust from two soils collected on the Namibian gravel plains. This is in agreement of the indications of the emission maps (Fig. 2), showing significant emissions in the gravel plains. The absence of seasonal cycle in the elemental composition illustrated in Figure S3 suggests that the seasonal change from northern to southern sources does not induce a change in the composition of the aerosol dust sampled at HBAO, which is consistent with the fact that the northern and the southern gravel plains of Namibia have similar mineralogy (Heine and Vökel, 2010). This suggests that the mineralogical composition of mineral dust should not be a discriminating factor explaining the seasonality of the iron solubility observed at HBAO.

4.2. Evidence of processing by marine biogenic emissions

The atmospheric (in-cloud) processing associated with secondary aerosol production may increase the fractional solubility of Fe during transport (Takahashi et al., 2011; Rodríguez et al., 2021). This has also been shown for Al and Ti (Baker et al., 2020). The chemical processing could include both acidic and ligand-promoted dissolution (Desboeufs et al., 2001, Longo et al., 2016, Tao et al., 2019). Oxalic acid has previously been used as a proxy for organic ligand–mediated iron dissolution processes because it is the most abundant species in the atmosphere and is the most effective ligand in promoting iron dissolution (Baker et al., 2020; Hamilton et al., 2021). However, several secondary compounds, such as carboxylate ligands and marine secondary products derived from DMS oxidation, have been identified as playing a role in increasing the soluble fraction of iron from mineral aerosols (Johansen and Key, 2006; Paris et al., 2011; Paris and Desboeufs, 2013; Wozniak et al., 2013 and 2015). The increase of ligands-promoted dissolution is attributed to photochemical reduction of Fe(III) in Fe (II) (Siefert et al., 1994; Johansen and Key, 2006).

To investigate these aspects, the mass concentrations of the ionic compounds (oxalate, formate, MSA, NO_3^-, NH_4^+ and nss-SO_4^{2-}) implied in the secondary aerosol production, measured at HBAO during dust and background periods are reported in Table 3**.**

Table 3. Average and standard deviations of mass concentrations of water-soluble ions measured at HBAO during dust and background events from May to December 2017. Concentrations are expressed in ng m^{-3}. The number of samples pertaining to each occurrence is indicated in brackets.

	Dust	**Background**
nss-SO_4^{2-}	1795 ± 762 (N = 42)	1366 ± 505 (N=132)
Oxalate	155 ± 53 (N = 42)	127 ± 35 (N = 132)
Formate	18 ± 6 (N = 40)	16 ± 9 (N = 105)
MSA	64 ± 37 (N=36)	56 ± 36 (N=114)
NO_3^-	205 ± 79 (N=42)	200 ± 138 (N=132)
NH_4^+	192 ± 71 (N=42)	207 ± 98 (N=132)

Oxalate was the most abundant organic compound, followed by MSA, a secondary product of DMS oxidation and a unique particulate tracer of the primary marine biogenic activity (Andreae et al., 1995). On average, organic compounds were equally concentrated in dust and background events. Amongst inorganic species, nss-SO_4^{2-} was the most concentrated compound, with higher values during the dust events than during the background period.

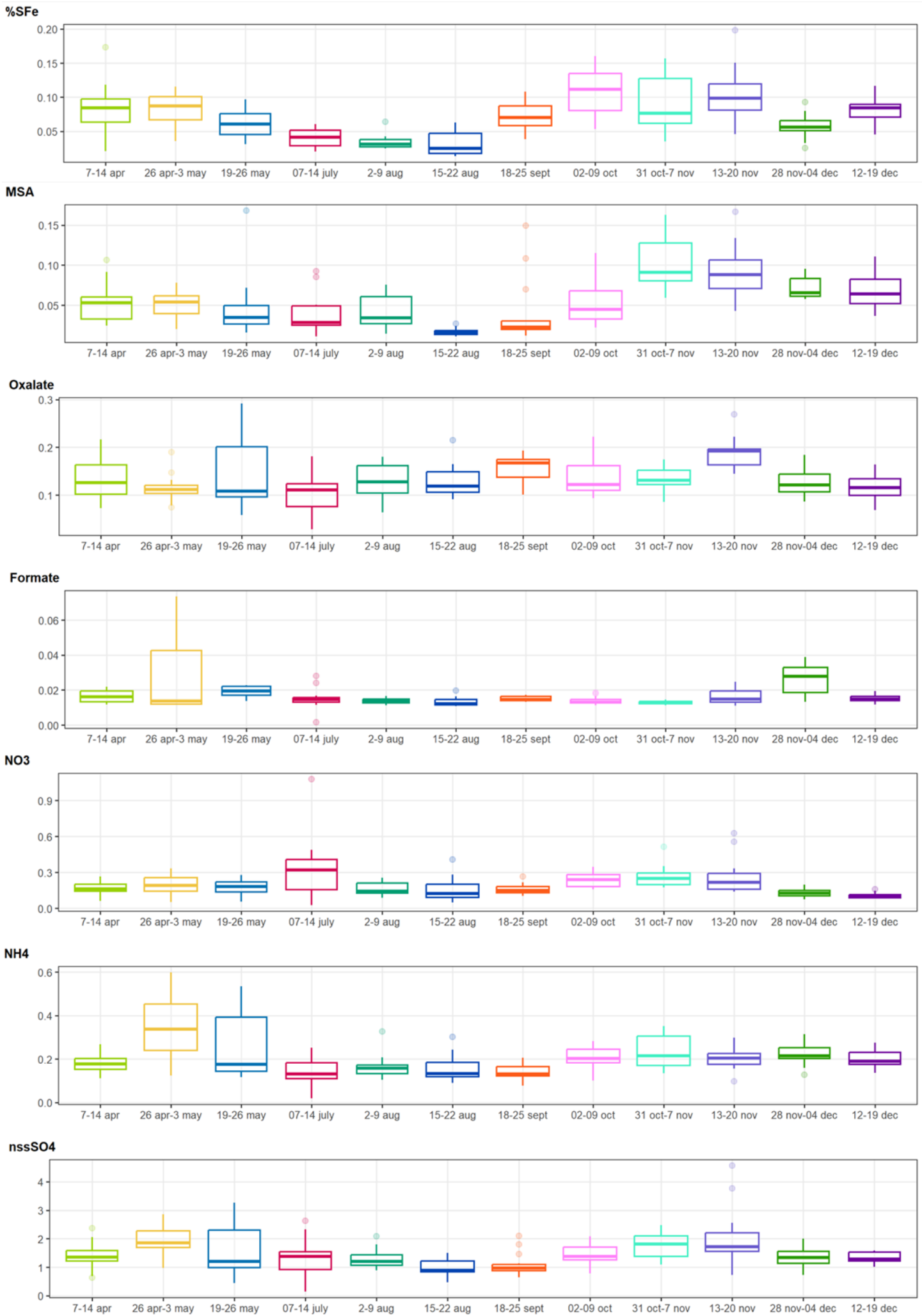
%SFe
0.20
0.15
0.10
0.05
MSA
0.15
0.10
0.05
Oxalate
0.3
0.2
0.1
Formate
0.06
0.04
0.02
0.00
NO3
0.9
0.6
0.3
0.0
NH4
0.6
0.4
0.2
0.0
nssSO4
4
3
2
1
0
7-14 apr
26 apr-3 may
19-26 may
07-14 july
2-9 aug
15-22 aug
18-25 sept
02-09 oct
31 oct-7 nov
13-20 nov
28 nov-04 dec
12-19 dec

Figure 6: Box-plots of the averages of %SFe and secondary organic and inorganic compounds mass concentrations (µg m^{-3}) for the sampling periods including all the samples (dust + background). Boxes and whiskers as in Fig. 3.

The detailed time series of secondary compounds are shown in Fig. 6, where they are compared to that of the %SFe. There is no clear seasonal cycle for any of the ionic compounds, with the exception of MSA, which shows a similar time variability than %SFe. MSA concentrations were lowest between May and August (average 38.0 ± 28.0 ng m^{-3}), while higher concentrations were measured from September to December (72.7 ± 38.1 ng m^{-3}). These differences are also observed for the dust cases only. The average MSA concentration was 40.6 ± 23.4 ng m^{-3} for Dust 04 to Dust 08 episodes. It increased to 77.7 ± 35.3 ng m^{-3}, almost a factor of 2 between episodes Dust 09 and Dust 13. The mass concentrations and the seasonal cycle of MSA are related with the proximity of the strong coastal upwelling by the Benguela current (Formenti et al., 2019; KL20). The maximum concentration of MSA (106.2 ng m^{-3}) was measured during episode Dust 11, which is also the time of the highest SFe% observation. This episode was also characterised by the highest oxalate, nss-SO_4^{2-} and NO_3^- concentrations. However, no clear correlation between the %SFe and the secondary compounds concentrations can be found in our data (Fig. S4). In order to statistically explore the potential links between %SFe and various parameters, Figure 7 shows the correspondence plot between total Fe, Al and Si, and their respective fractional solubility, the measured secondary compounds and the meteorological conditions during sampling obtained from Principal Component Analysis (PCA) for all the samples. The variables correlated in time are grouped together (the closer they are in the circle, the stronger the correlation) whereas the variables which are anti-correlated are situated on the opposite side of the plot origin.

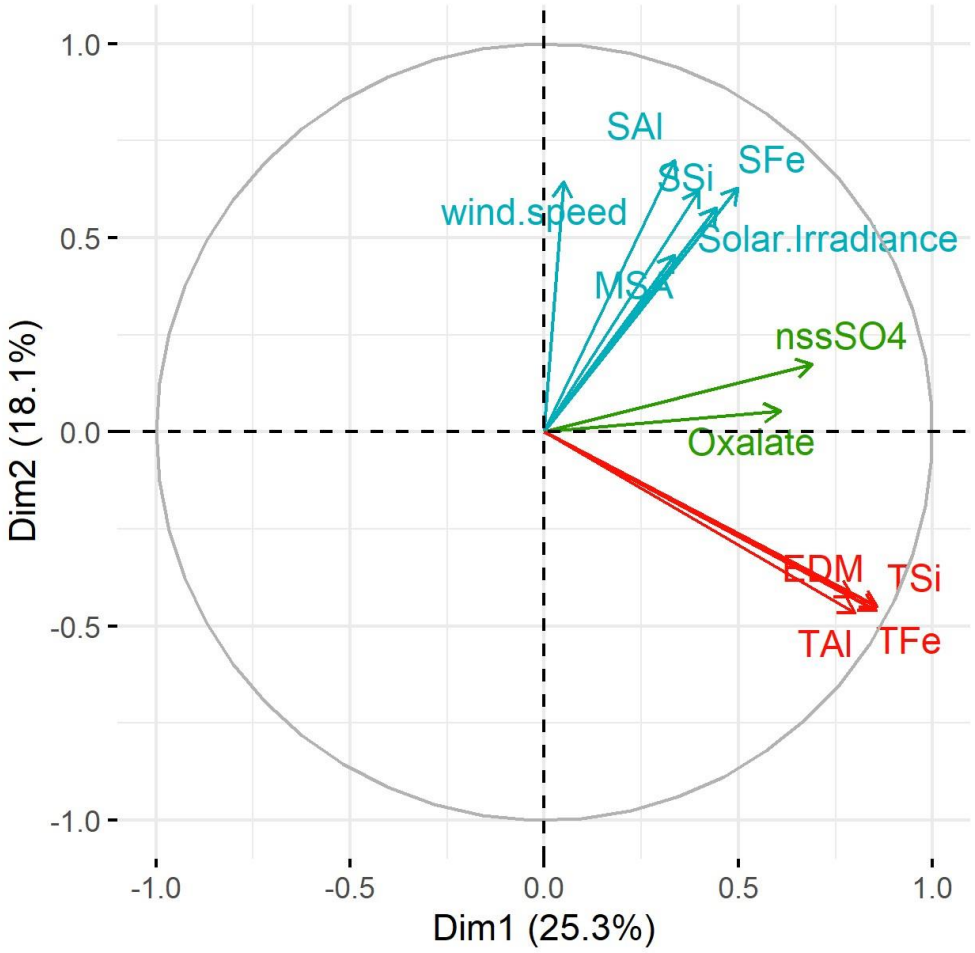

Figure 7: PCA analysis performed from the database including %SX,TX, EDM, secondary ions concentrations and meteorological parameters. The colour of variables by groups is defined by a clustering algorithm, tending to find clusters of comparable spatial extent. Each colour corresponds to a cluster of parameters which evolve in the same way. Formate, nitrate, ammonium, acetate, humidity, and wind speed are not visible in the plot showing that they are not significantly correlated with the other parameters (i.e. their squared cosine < 0.4).

The PCA plot (Fig. 7) emphasizes 3 groups of dependent parameters: 1. a high correlation between total Fe, Al and Si concentrations and dust loading (EDM), as previously identified in Table 1 and Fig. 3, 2. a relation between oxalate and nss-SO_4^{2-} concentrations, suggesting a common chemical process of formation, and 3.the dependence between %SFe (%SAl and %SSi), the MSA concentrations, the solar irradiance and to a lesser extent with the wind speed. While it is expected that the emission of mineral dust occurs when the wind speed is high, the correlation of %SFe with wind speed is rather surprising since the %SFe is independent of the dust load (Fig. 2 and 7). Figures S4 in the supplementary material present the plots between %SFe, MSA concentrations, solar irradiance and wind speed for background and dust events. The correlation between the wind speed and the MSA concentrations (Fig. S4) is consistent with Andreae et al. (1995), who demonstrated how, in this area

due to persistent phytoplankton bloom, the atmospheric concentrations of DMS, the gaseous precursors of MSA, depend on the sea-to-air flux, in turn is determined by the concentrations in the ocean water and the surface wind speed.

As previously mentioned, Johansen and Key (2006) showed an increase of dissolution of ferrihydrite, a proxy of iron(oxy)hydroxide found in desert mineral dust, by photolysis of the Fe(III)-MSIA (methane sulfinic acid) complex, producing MSA and soluble Fe. Zhuang et al. (1992) proposed an increase of iron dissolution by the acidification of aerosol particles associated with DMS oxidation. Here, the link between the %SFe, solar irradiance and MSA is in agreement with the photo-reduction dissolution of Fe by MSA condensation on Fe-bearing dust. Thus, we attribute the %SFe seasonality observed at HBAO both to solar irradiance and MSA temporal evolution via this process. It is interesting to note that due to the high correlation between %SFe and %SAl and %SSi, the photochemical processes could also impact the solubility of all element-bearing dust.

4.3. Link to other sources of iron and oxalate

Formenti et al. (2018) have shown that in the Austral winter, when the synoptic circulation is dominantly anti-cyclonic, air masses laden with light-absorbing aerosols either from ship pollution or biomass burning can be transported to HBAO (Formenti et al., 2018). However, the lowest Fe solubility (< 5%) was measured in July and August 2017, and no correlation between the %SFe and the percent mass fraction of iron from sources other than dust can be found in our data (not shown).

The mass apportionment of iron reported by KL20 indicates that, during the dust events and the background periods, respectively, 7% and 29% of the mass of total elemental Fe was not associated to mineral dust, but rather to a factor indicated as “ammonium-neutralised component”, mostly characterised by secondary species, and non-sea-salt potassium ($nss\text{-}K^{+}$). The PMF (Positive Matrix Factorisation) analysis indicated that the “ammonium-neutralised component” was associated to photo-oxidation of marine biogenic emission but also episodically to biomass burning. This component includes oxalate, the most concentrated organic species at HBAO, and the strongest of the organic ligands promoting the photo-reduction of iron in mineral dust, henceforth the increase of its fractional solubility (Paris and Desboeufs, 2013). Surprisingly, excepted individual cases (Dust 13), our analysis does not show this strong link (Fig. 7), and indeed, contrary to the SFe%, the oxalate concentrations measured at HBAO was practically constant with time (in average 0.14+/- 0.04 $\mu g.m^{-3}$). The possible pathways of oxalate formation in this complex atmosphere are numerous through the year, from natural and anthropogenic sources (marine, heavy-oil combustion, biomass burning) and in-cloud and photo-oxidative processes (Baboukas et al., 2000; Myriokefalitakis et al., 2011).

5. Concluding remarks

For the first time, the fractional solubility of Fe in airborne atmospheric aerosols smaller than 10 µm in diameter is investigated along the west coast of Namibia, in southern Africa, a critical region for the global climate.

Ten intense episodes of transport of mineral dust from aeolian erosion were identified from the analysis of aerosol samples collected between May and December 2017 at the Henties Bay Aerosol Observatory (HBAO). Based on modelling and measurements, source regions were identified both in the northern and southern gravel plans. Our data do not provide any evidence of the possible contribution of dust from coastal riverbeds, which are considered to be frequent sources of atmospheric dust and soluble iron in the region (Vickery et al., 2013; Von Holdt et al., 2017; Dansie et al., 2017a; 2017b). The total iron represents, on average, 5.8 % (± 0.6 %) of the total dust mass, and that the average water-soluble Fe fractional solubility is 6.9 % (± 3.3 %). These values should be useful to atmospheric models estimating the dust-borne input of soluble Fe from the gravel plains in Namibia to the surrounding oceans.

The seasonal increase of the %SFe is associated to that of the concentrations of MSA and correlated to meteorological parameters such as the wind speed and the surface solar irradiance. Our observations support the role of photo-chemical processes in the dissolution of Fe in our samples, and suggest that the oxidation of the marine biogenic emissions from the northern Benguela upwelling, favoured under high wind speed conditions, could play a significant role in increasing the solubility of elemental iron in mineral dust aerosols over coastal Namibia. This is in agreement with the mechanism described by Zhuang et al. (1992), who proposed an increase of iron dissolution by the acidification of aerosol particles associated with DMS oxidation, and Johansen and Key (2006), who showed an increase of dissolution of ferrihydrite, a proxy of iron(oxy)hydroxide found in desert mineral dust, by photolysis of the Fe(III)-MSIA (methane sulfinic acid) complex, producing MSA and soluble Fe. It is interesting to note that due to the high correlation between %SFe, %SAl and %SSi (and %STi), the same photochemical processes could also impact the solubility of all element-bearing dust. The possible mechanism suggested by this paper could be responsible for initiating a feedback loop whereby the input of dust of increased trace and major elements solubility would result in stronger marine biogenic emissions to the atmosphere. This possible mechanism could increase the iron solubility in mineral dust, maybe also initiating a feedback loop whereby the input of dust of increased solubility would result in stronger marine biogenic emissions to the atmosphere, including Volatile Organic Compounds, in particular butene, massively emitted by the organisms in the coastal marine foam (Giorio et al., 2022).This complex and dynamic environment where the interplay between the input of atmospheric iron from transported dust and the marine biogenic emissions from the Benguela oceanic upwelling system should be further addressed by future research.

Data availability. Atmospheric concentrations of total and dissolved elements and water-soluble ions measured over coastal Namibia in 2017 are available in the Easy Data (Formenti et al., 2023, https://doi.org/10.57932/2ac79cd1-282a-4004-87d5-38f0ebcaf40c). The statistical FactoMineR package is available in R (R version 4.1.2, 2021; http://factominer.free.fr/index_fr.html, last accessed 20/07/2023). Meteorological data from the Wlotzkasbaken station (22.31°S, 14.45°E, 73 m asl) are part of the Southern African Science Service Centre for Climate Change and Adaptive Land Management (SASSCAL) ObservationNet (https://www.sasscal.org/; last accessed 14/04/2023).

Author contributions. PF, DK, SJP, AN, MC, AF and SC prepared and performed the filter sampling. RT, KD, PF, SC, ST,and CMB performed the XRF, IC and ICP analysis of the collected samples. BL performed the field implementation. KS and SF performed the model calculations of dust emission fluxes. JPC performed the model calculations of air mass back-trajectories. HA and JC provided with the satellite retrieval of fog and low clouds. PF, KD, RT and SJP analysed and interpreted the dataset. PF and KD wrote the paper with contributions from RT and SJP, and the remaining authors. PF and SJP provided funding. PF coordinated the research activity and supervised its planning and execution.

Competing interests. PF is guest editor for the ACP Special Issue “New observations and related modelling studies of the aerosol–cloud–climate system in the Southeast Atlantic and southern Africa regions”. The remaining authors declare that they have no conflicts of interests.

Special issue statement. This article is part of the special issue “New observations and related modelling studies of the aerosol–cloud–climate system in the Southeast Atlantic and southern Africa regions (ACP/AMT inter-journal SI)”. It is not associated with a conference.

Acknowledgements. This work receives funding by the French Centre National de la Recherche Scientifique (CNRS) and the South African National Research Foundation (NRF) through the “Groupement de Recherche Internationale Atmospheric Research in southern Africa and the Indian Ocean” (GDRI-ARSAIO) and the Project International de Coopération Scientifique (PICS) “Long-term observations of aerosol properties in Southern Africa” (contract n. 260888) as well as by the Partenariats Hubert Curien (PHC) PROTEA of the French Minister of Foreign Affairs and International Development (contract numbers 33913SF and 38255ZE). D. Klopper acknowledges the financial support of the Climatology Research Group of North-West University and the travel scholarship of the French Embassy in South Africa (internship at LISA in summer 2018). R. Torres-Sánchez acknowledges the

572 Postdoctoral Fellowship Margarita Alsolas (University of Huelva) funded by the Ministry of Universities
573 of Spain (NextGenerationEU). The Southern African Science Service Centre for Climate Change and
574 Adaptive Land Management (SASSCAL) ObservationNet (https://www.sasscal.org/) is acknowledged
575 for open-access data provision. The authors would also like to acknowledge the support by the IPGP
576 platform PARI for HR-ICP-MS analysis. F. Lahmidi and Z. Zeng (LISA) are acknowledged for support
577 to the ion chromatography analysis.
578

References

Andersen, H. and Cermak, J.: First fully diurnal fog and low cloud satellite detection reveals life cycle in the Namib, Atmos. Meas. Tech., 11, 5461–5470, doi: 10.5194/amt-11-5461-2018, 2018.

Andersen, H., Cermak, J., Solodovnik, I., Lelli, L. and Vogt, R.: Spatiotemporal dynamics of fog and low clouds in the Namib unveiled with ground- and space-based observations, Atmos. Chem. Phys., 1, 4383–4392, doi: 10.5194/acp-19-4383-2019, 2019.

Andersen, H., Cermak, J., Fuchs, J., Knippertz, P., Gaetani, M., Quinting, J., Sippel, S., and Vogt, R.: Synoptic-scale controls of fog and low-cloud variability in the Namib Desert, Atmos. Chem. Phys., 20, 3415–3438, https://doi.org/10.5194/acp-20-3415-2020, 2020.

Andreae, M. O.: Soot Carbon and Excess Fine Potassium: Long-Range Transport of Combustion-Derived Aerosols, Science, 220, 1148-1151, doi:10.1126/science.220.4602.1148, 1983.

Andreae, M. O., Elbert, W., and de Mora, S. J.: Biogenic sulfur emissions and aerosols over the tropical South Atlantic: 3. Atmospheric dimethylsulfide, aerosols and cloud condensation nuclei, J. Geophys. Res., 100, 11335-11356, https://doi.org/10.1029/94JD02828, 1995.

Annegarn, H.J., van Grieken, R.E., Bibby, D.M. and von Blottnitz, F.: Background Aerosol Composition in the Namib Desert, South West Africa (Namibia), Atmos. Environ., 17, 2045–2053, doi: 10.1016/0004-6981(83)90361-X, 1983.

Bhattachan, A., D'Odorico, P., Baddock, M.C., Zobeck, T.M., Okin, G.S., Cassar, N.: The Southern Kalahari: a potential new dust source in the Southern hemisphere?, Environ. Res. Lett., 7, 024001. http://dx.doi.org/10.1088/1748-9326/7/2/024001, 2012.

Bhattachan, A., P. D'Odorico, and G. S. Okin, Biogeochemistry of dust sources in Southern Africa, J. Arid Environ., 117, 18-27, http://dx.doi.org/10.1016/j.jaridenv.2015.02.013, 2015.

Baboukas, E. D., Kanakidou, M., and Mihalopoulos, N.: Carboxylic acids in gas and particulate phase above the Atlantic Ocean, J. Geophys. Res., 105, 14459–14471, https://doi.org/10.1029/1999JD900977, 2000.

Baker A.R., T. D. Jickells, M. Witt, and K. L. Linge, Trends in the solubility of iron, aluminium, manganese and phosphorus in aerosol collected over the Atlantic Ocean., Marine Chem., 98, 43-58, https://doi.org/10.1016/j.marchem.2005.06.004, 2006.

Baker, A. R., and T. D. Jickells, Mineral particle size as a control on aerosol iron solubility, Geophys. Res. Lett., 33, L17608. https://doi.org/10.1029/2006GL026557, 2006.

Baker, A. R., C. Adams C., T. G. Bell, T. D. Jickells, and L. Ganzeveld, Estimation of atmospheric nutrient inputs to the Atlantic Ocean from 50°N to 50°S based on large-scale field sampling: iron and other dust-associated elements, Glob. Biogeochem. Cycles, 27, 755–767, doi:10.1002/gbc.20062, 2013.

Baker, A. R., M. Thomas, H. W. Bange, and E. Plasencia Sánchez, E., Soluble trace metals in aerosols over the tropical south-east Pacific offshore of Peru, Biogeosciences, 13, 817–825, https://doi.org/10.5194/bg-13-817-2016, 2016.

Baker, Alex R., et T. D. Jickells, Atmospheric deposition of soluble trace elements along the Atlantic Meridional Transect (AMT), in *The Atlantic Meridional Transect programme (1995-2016)* 158: 41-51. https://doi.org/10.1016/j.pocean.2016.10.002, 2017.

Baker, A. R., M. Li, and R. Chance, Trace metal fractional solubility in size-segregated aerosols from the tropical eastern Atlantic Ocean, Global Biogeochemical Cycles, 34, e2019GB006510. https://doi.org/10.1029/2019GB006510, 2020.

Bryant, R. G., Bigg, G. R., Mahowald, N. M., Eckardt, F. D., and Ross, S. G., Dust emission response to climate in southern Africa, J. Geophys. Res., 112, D09207, doi:10.1029/2005JD007025, 2007.

Caponi, L., Formenti, P., Massabó, D., Di Biagio, C., Cazaunau, M., Pangui, E., Chevaillier, S., Landrot, G., Andreae, M. O., Kandler, K., Piketh, S., Saeed, T., Seibert, D., Williams, E., Balkanski, Y., Prati, P., and Doussin, J.-F.: Spectral- and size-resolved mass absorption efficiency of mineral dust aerosols in the shortwave spectrum: a simulation chamber study, Atmos. Chem. Phys., 17, 7175–7191, https://doi.org/10.5194/acp-17-7175-2017, 2017.

Chaboureau, J.-P., L. Labbouz, C. Flamant, and A. Hodzic. Acceleration of the southern African easterly jet driven by radiative effect of biomass burning aerosols and its impact on transport during AEROCLO-sA, Atmos. Chem. Phys.,22, 8639-8658, https://doi.org/10.5194/acp-22-8639-2022, 2022.

Chance R, T. D. Jickells and A. R. Baker, Atmospheric trace metal concentrations, solubility and deposition fluxes in remote marine air over the south-east Atlantic, Marine Chemistry, 177, 45–56, doi:10.1016/j.marchem.2015.06.028, 2015.

Dansie, A. P., G. F. S. Wiggs, D. S. G. Thomas, and R. Washington, Measurements of windblown dust characteristics and ocean fertilisation potential: The ephemeral river valleys of Namibia, Aeolian Res., 29, 30–41, doi:10.1016/j.aeolia.2017.08.002, 2017a.

Dansie, A. P., G. F. S. Wiggs, and D. S. G. Thomas, Iron and nutrient content of wind-erodible sediment in the ephemeral river valleys of Namibia, Geomorphology, 290, 335-346, https://doi.org/10.1016/j.geomorph.2017.03.016, 2017b.

Dansie AP, Thomas DSG, Wiggs GFS, Baddock MC, Ashpole I. Plumes and blooms - Locally-sourced Fe-rich aeolian mineral dust drives phytoplankton growth off southwest Africa. Sci Total Environ., doi: 10.1016/j.scitotenv.2022.154562, 2022.

Desboeufs, K. V., R. Losno, et J. L. Colin, Factors influencing aerosol solubility during cloud processes, Atmos. Environ., 35, 3529-3537, https://doi.org/10.1016/S1352-2310(00)00472-6, 2001.

Desboeufs, K.V., Sofikitis, A., Losno, R., Colin, J.L., Ausset, P. Dissolution and solubility of trace metals from natural and anthropogenic aerosol particulate matter, Chemosphere 58, 195–203, 2005.

Desboeufs, K., Fu, Y., Bressac, M., Tovar-Sánchez, A., Triquet, S., Doussin, J.F., Giorio, C., Chazette, P., Disnaquet, J., Feron, A., Formenti, P., Maisonneuve, F., Rodríguez-Romero, A., Zapf, P., Dulac, F., and Guieu, C., Wet deposition in the remote western and central Mediterranean as a source of trace metals to surface seawater, Atmos. Chem. Phys., 22, 2309–2332, https://doi.org/10.5194/acp-22-2309-2022, 2022.

Eltayeb, M.A.; Van Grieken, R.E., Maenhaut, W. and Annegarn, H.J.: Aerosol-Soil Fractionation for Namib Desert Samples. Atmos. Environ., 27(5), https://doi.org/10.1016/0960-1686(93)90185-2, 1993.

Feuerstein, S., and Schepanski, K.: Identification of Dust Sources in a Saharan Dust Hot-Spot and Their Implementation in a Dust-Emission Model, Remote Sensing, 11, doi:10.3390/rs110100004, 2019.

Flamant, C., M. Gaetani, J.-P. Chaboureau, P. Chazette, S. J. Piketh, and P. Formenti. Smoke in the river: an Aerosols, Radiation and Clouds in southern Africa (AEROCLO-sA) case study, Atmos. Chem. Phys., 22, 5701–5724, https://doi.org/10.5194/acp-22-5701-2022, 2022.

Formenti, P., Schütz, L., Balkanski, Y., Desboeufs, K., Ebert, M., Kandler, K., Petzold, A., Scheuvens, D., Weinbruch, S., and Zhang, D.: Recent progress in understanding physical and chemical properties of African and Asian mineral dust, Atmos. Chem. Phys., 11, 8231–8256, https://doi.org/10.5194/acp-11-8231-2011, 2011.

Formenti, P., S. Caquineau, K. Desboeufs, A. Klaver, S. Chevaillier, E. Journet, J. L. Rajot, Mapping the physico-chemical properties of mineral dust in western Africa: mineralogical composition, Atmos. Chem. Phys., 14, 10663-1068, 2014.

Formenti, P., Piketh, S. J., Namwoonde, A., Klopper, D., Burger, R., Cazaunau, M., Feron, A., Gaimoz, C., Broccardo, S., Walton, N., Desboeufs, K., Siour, G., Hanghome, M., Mafwila, S., Omoregie, E., Junkermann, W., and Maenhaut, W.: Three years of measurements of light-absorbing aerosols over coastal Namibia: seasonality, origin, and transport, Atmos. Chem. Phys., 18, 17003-17016, https://doi.org/10.5194/acp-18-17003-2018, 2018.

Formenti, P., B. D'Anna, C. Flamant, M. Mallet, S.J. Piketh, K. Schepanski, F. Waquet, F. Auriol, G. Brogniez, F. Burnet, J. Chaboureau, A. Chauvigné, P. Chazette, C. Denjean, K. Desboeufs, J. Doussin, N. Elguindi, S. Feuerstein, M. Gaetani, C. Giorio, D. Klopper, M.D. Mallet, P. Nabat, A. Monod, F. Solmon, A. Namwoonde, C. Chikwililwa, R. Mushi, E.J. Welton, and B. Holben, The Aerosols, Radiation and Clouds in Southern Africa Field Campaign in Namibia: Overview, Illustrative Observations, and Way Forward, Bull. Amer. Meteor. Soc., 100, 1277–1298, https://doi.org/10.1175/BAMS-D-17-0278.1, 2019.

Gao, Y., Xu, G., Zhan, J., Zhang, J., Li, W., Lin, Q., Chen, L., and Lin, H., Spatial and particle size distributions of atmospheric dissolvable iron in aerosols and its input to the Southern Ocean and coastal East Antarctica, J. Geophys. Res., 118, 12,634–12,648, doi:10.1002/2013JD020367, 2013.

Gili, S., Vanderstraeten, A., Chaput, A., King, J., Gaiero, D. M., Delmonte, B., Vallelonga, Paola Formenti, Claudia Di-Biagio, Mathieu Cazaunau, Edouard Pangui, Jean-Francois Doussin, Mattielli, N., South African dust contribution to the high southern latitudes and East Antarctica during interglacial stages, Communications Earth & Environment, 3, 129, https://doi.org/10.1038/s43247-022-00464-z, 2022.

Ginoux, P., Prospero, J.M., Gill, T.E., Hsu, N.C., Zhao, M.: Global-scale attribution of anthropogenic and natural dust sources and their emission rates based on MODIS Deep Blue aerosols products, Rev. Geophys., 50, RG3005, doi:10.1029/2012RG000388, 2012.

Giorio, C., Doussin, J.F., D'Anna, B., Mas, S., Filippi, D., Denjean, C., Mallet,M.D., Bourrianne,T., Burnet, F, Cazanaur,M., Chikwililwa, C., Desboeufs, K., Feron, A., Michoud, V., Namwoonde, A., Andreae, M.O., Piketh,

687 S.J. and Formenti, P.: Butene emissions from coastal ecosystems may contribute to new particle formation,
688 Geophys. Res. Lett., 49, https://doi.org/10.1029/2022GL098770, 2022.

689 Grini, A., Tulet, P., and Gomes, L.: Dusty weather forecasts using the MesoNH mesoscale atmospheric model.
690 J. Geophys. Res., 111, D19205, https://doi.org/10.1029/2005JD007007, 2006.

691 Hamilton, D. S., Perron, M.M.G., Bond, T.C., Bowie, A.R., Buchholz, R.R., Guieu, C., Ito, A., Maenhaut, W.,
692 Myriokefalitakis, S., Olgun, N., Rathod, S.D., Schepanski, K., Tagliabue, A., Wagner, R. and Mahowald, N.M.:
693 Earth, wind, fire, and pollution: Aerosol nutrient sources and impacts on ocean biogeochemistry, Annual re-
694 view of Marine Science, 14, pp. 303- 330, https://doi.org/10.1146/annurev-marine-031921-013612, 2021.

695 Heike, K and J. Volkel, Soil clay minerals in Namibia and their significance for the terrestrial and marine past
696 global change, African Study Monographs, Suppl.40, 2010.

697 Heimburger, A., Losno, R., and Triquet, S.: Solubility of iron and other trace elements in rainwater collected on
698 the Kerguelen Islands (South Indian Ocean), Biogeosciences, 10, 6617–6628, https://doi.org/10.5194/bg-10-
699 6617-2013, 2013.

700 Hooper, H., Mayewski, P., Marx, S., Henson, S., Potocki, M., Sneed, S., Handley, M., Gasso, S., Fischer, M.,
701 Saunders, K.M., Examining links between dust deposition and phytoplankton response using ice cores. Aeo-
702 lian Res., 36, 45-60, https://doi.org/10.1016/j.aeolia.2018.11.001, 2019.

703 Ito, A., and Kok, J. F.: Do dust emissions from sparsely vegetated regions dominate atmospheric iron supply to
704 the Southern Ocean?, J. Geophys. Res., 122, 3987-4002, https://doi.org/10.1002/2016JD025939, 2017.

705 Ito, A., Y. Ye, C. Baldo, and Z. Shi, Ocean Fertilization by Pyrogenic Aerosol Iron. npj Climate Atmos. Sci., 4,
706 30, doi: 10.1038/s41612-021-00185-8, 2021.

707 Jickells, T., Andersen, K.K., Baker, A., Bergametti, G., Brooks, N., Cao, J., Boyd, P., Duce, R., Hunter, K.,
708 Global iron connections between desert dust, ocean biogeochemistry, and climate, Science, 308, 67-71, DOI:
709 10.1126/science.1105959, 2005.

710 Journet, E., Desboeufs, K., Caquineau, S. and Colin, J. L.: Mineralogy as a critical factor of dust iron solublity,
711 Geophys. Res. Lett., 35, https://doi.org/10.1029/2007GL031589, 2008.

712 Johansen, A. M., and Key, J. M.: Photoreductive dissolution of ferrihydrite by methanesulfinic acid: Evidence of
713 a direct link between dimethylsulfide and iron-bioavailability, Geophys. Res. Lett., 33, L14818,
714 doi:10.1029/2006GL026010, 2006.

715 Kaplan, J.O., Bigelow, N.H., Prentice, I.C., Harrison, S.P., Bartlein, P.J., Christensen, T.R., Cramer, W., Matve-
716 yeva, N.V., McGuire, A.D., Murray, D.F., Razzhivin, V.Y., Smith, B., Walker, D.A., Anderson, P.M., Andreev,
717 A.A., Brubaker, L.B., Edwards, M.E. and Lozhkin A.V.: Climate change and Arctic ecosystems: 2. Modeling,
718 paleodata-model comparison and future projections, J. Atmos. Res., 108, 8171, doi: 10.1029/2002JD002559,
719 2003.

720 Kangueehi, K. I., Southern African dust characteristics and potential impacts on the surrounding oceans, PhD
721 Thesis, Stellenbosch University, http://hdl.handle.net/10019.1/123923, 2021.

722 Klopper, D., Formenti, P., Namwoonde, A., Cazaunau, M., Chevaillier, S., Feron, A., Gaimoz, C., Hease, P.,
723 Lahmidi, F., Mirande-Bret, C., Triquet, S., Zeng, Z. And Piketh, S.J.: Chemical composition and source appor-
724 tionment of atmospheric aerosols on the Namibian Coast, Atmos. Chem. Phys., 20, pp. 15811 – 15833,
725 https://doi.org/10.5194/acp-20-15811-2020, 2020.

726 Kok, J. F., Albani, S., Mahowald, N. M., and Ward, D. S.: An improved dust emission model – Part 2: Evaluation
727 in the Community Earth System Model, with implications for the use of dust source functions, Atmos. Chem.
728 Phys., 14, 13043–13061, https://doi.org/10.5194/acp-14-13043-2014, 2014.

729 Kok, J.F., Ridley, D.A., Zhou, Q., Miller, R.L., Zhao, C., Heald, C.L., Ward, D.S., Albani, S., Haustein, K.: Smaller
730 desert dust cooling effect estimated from analysis of dust size and abundance. Nature Geoscience, 10, 274–
731 278, https://doi.org/10.1038/ngeo2912, 2017.

732 Laurent, B., Marticorena, B., Bergametti, G., Chazette, P., Maignan, F. and Schmechtig C.: Simulation of the
733 mineral dust emission frequencies from desert areas of China and Mongolia using an aerodynamic roughness
734 length map derived from POLDER/ADEOS 1 surface products, J. Geophys. Res., 110, D18, doi:
735 10.1029/2004JD005013, 2005.

736 Lide, D. R.: CRC Handbook of Chemistry and Physics 1991–1992, CRC Press, Boca Raton, Florida, 1992.

737 Liu, M., Matsui, H., Hamilton, D.S., Lamb, K.D., Rathod, S.D., Schwarz, J.P. and Mahowald, N.M.: The underap-
738 preciated role of anthropogenic sources in atmospheric soluble iron flux to the Southern Ocean, Climate At-
739 mos. Sci., 5, 28, https://doi.org/10.1038/s41612-022-00250-w, 2022.

740 Longo, A., F. Y. Feng, B., W. M. Landing, R.U. Shelley, A. Nenes, N. Mihalopoulos, K. Violaki, E. D. Ingall.
741 Influence of Atmospheric Processes on the Solubility and Composition of Iron in Saharan Dust, Environ. Sci.
742 Tech., 50, 13: 6912-20. https://doi.org/10.1021/acs.est.6b02605, 2016.

743 Mahowald, N., Luo, C., del Corral, J., Zender, C.S.: Interannual variablity in atmospheric mineral aerosols from
744 a 22-year model simulation and observational data, J. Geophys. Res., 108 (D12),
745 https://doi.org/10.1029/2002JD002821, 2003.

746 Marcotte, A.R., Anbar, A.D., Majestic, B.J., Herckes, P.: Mineral dust and iron solubility: Effects of composition,
747 particle size, and surface area, Atmosphere, 11, 533, doi:10.3390/atmos11050533, 2020.

748 Marticorena, B. and Bergametti, G.: Modelling the atmospheric dust cycle: 1. Design of a soil-derived dust
749 emission scheme, J. Geochem. Res., 16415-16430, 1995.

750 Marticorena, B., Chazette, P., Bergametti, G., Dulac, F., Legrand, M.: Mapping the aerodynamic roughness
751 length of desert surfaces from the POLDER/ADEOS bi-directional reflectance product, Int. J. Remote Sens.,
752 25, 603– 626, 2004.

753 Myriokefalitakis, S., Tsigarid is, K., Mihalopoulos, N., Scia re, J., Nenes, A., Kawamura,K., Segers, A., and
754 Kanakidou, M.: In-cloud oxalate formation in the global troposphere: a 3-D modeling study, Atmos. Chem.
755 Phys., 11, 5761-5782, doi:10.5194/acp-11-5761-2011, 2011.

Paris, R., Desboeufs, K. V., Formenti, P., Nava, S., and Chou, C.: Chemical characterisation of iron in dust and biomass burning aerosols during AMMA-SOP0/DABEX: implication for iron solubility, Atmos. Chem. Phys., 10, 4273–4282, https://doi.org/10.5194/acp-10-4273-2010, 2010.

Paris, R., K.V. Desboeufs, et E. Journet. Variability of dust iron solubility in atmospheric waters: Investigation of the role of oxalate organic complexation, Atmos. Environ., 45, 6510-17. https://doi.org/10.1016/j.atmosenv.2011.08.068, 2011.

Paris, R., and K. V. Desboeufs, Effect of atmospheric organic complexation on iron-bearing dust solubility. Atmos. Chem. Phys., 13, 4895-4905, https://doi.org/10.5194/acp-13-4895-2013, 2013.

Perron, M. M. G., Strzelec, M., Gault-Ringold, M., Proemse, B. C., Boyd, P. W., and Bowie, A. R.: Assessment of leaching protocols to determine the solubility of trace metals in aerosols, Talanta, 208, 120377, https://doi.org/10.1016/j.talanta.2019.120377, 2020.

Prospero, J.M., Ginoux, P., Torres, O., Nicholson S.E. and Gill, T.M.: Environmental characterization of global sources of atmospheric soil dust identified with the Nimbus 7 total ozone mapping spectrometer (TOMS) absorbing aerosol product. Reviews of Geophysics, 40 (1): 1002, https://doi.org/10.1029/2000RG000095, 2002.

Redemann, J., Wood, R., Zuidema, P., Doherty, S. J., Luna, B., LeBlanc, S. E., Diamond, M. S., Shinozuka, Y., Chang, I. Y., Ueyama, R., Pfister, L., Ryoo, J.-M., Dobracki, A. N., da Silva, A. M., Longo, K. M., Kacenelenbogen, M. S., Flynn, C. J., Pistone, K., Knox, N. M., Piketh, S. J., Haywood, J. M., Formenti, P., Mallet, M., Stier, P., Ackerman, A. S., Bauer, S. E., Fridlind, A. M., Carmichael, G. R., Saide, P. E., Ferrada, G. A., Howell, S. G., Freitag, S., Cairns, B., Holben, B. N., Knobelspiesse, K. D., Tanelli, S., L'Ecuyer, T. S., Dzambo, A. M., Sy, O. O., McFarquhar, G. M., Poellot, M. R., Gupta, S., O'Brien, J. R., Nenes, A., Kacarab, M., Wong, J. P. S., Small-Griswold, J. D., Thornhill, K. L., Noone, D., Podolske, J. R., Schmidt, K. S., Pilewskie, P., Chen, H., Cochrane, S. P., Sedlacek, A. J., Lang, T. J., Stith, E., Segal-Rozenhaimer, M., Ferrare, R. A., Burton, S. P., Hostetler, C. A., Diner, D. J., Seidel, F. C., Platnick, S. E., Myers, J. S., Meyer, K. G., Spangenberg, D. A., Maring, H., and Gao, L.: An overview of the ORACLES (ObseRvations of Aerosols above CLouds and their intEractionS) project: aerosol–cloud–radiation interactions in the southeast Atlantic basin, Atmos. Chem. Phys., 21, 1507–1563, https://doi.org/10.5194/acp-21-1507-2021, 2021.

Reichholf, J. H., Is Saharan Dust a Major Source of Nutrients for the Amazonian Rain Forest?, Studies on Neotropical Fauna and Environment, 21:4, 251-255, DOI: 10.1080/01650528609360710, 1986.

Rodríguez, S., Prospero, J.M., Lopez-Darias, J., Garcia-Alvarez, M.I., Zuidema, P., Nava, S., Lucarelli, F., Gaston, C.J., Galindo, L., Sosa, E.: Tracking the changes of iron solubility and air pollutants traces as African dust transits the Atlantic in the Saharan dust outbreaks. Atmos. Environ., 246, 118092, https://doi.org/10.1016/j.atmosenv.2020.118092, 2021.

Rodríguez, S., Riera, R., Fonteneau, A., Alonso-Pérez, S., and López-Darias, J.: African desert dust influences migrations and fisheries of the Atlantic skipjack-tuna, Atmospheric Environment, 312, 120022, https://doi.org/10.1016/j.atmosenv.2023.120022, 2023.

Shelley, R.U., Morton, P.L., Landing, W.M., Elemental ratios and enrichment factors in aerosols from the US-GEOTRACES North Atlantic transects. Deep-Sea Res. II, 2014.

Shelley, R. U., Landing, W. M., Ussher, S. J., Planquette, H., & Sarthou, G. Regional trends in the fractional solubility of Fe and other metals from North Atlantic aerosols (GEOTRACES cruises GA01 and GA03) following a two-stage leach, Biogeosciences, 15(8), 2271–2288. https://doi.org/10.5194/bg-15-2271-2018, 2018.

Sholkovitz, E.R., Sedwick, P.N., Church, T.M. Influence of anthropogenic combustion emissions on the deposition of soluble aerosol iron to the ocean: empirical estimates for island sites in the North Atlantic, Geochim. Cosmochim. Acta, 73, 3981–4003, http://dx.doi.org/10.1016/j.gca.2009.04.029, 2009.

Siefert, R. L., S. O. Pehkonen, Y. Erel, and M. R. Hoffman, Iron photochemistry of aqueous suspensions of ambient aerosol with added organic acids, Geochim. Cosmochim. Acta, 58, 3271–3279, 1994.

Spirig, R., Vogt, R., Larsen, J. A., Feigenwinter, C., Wicki, A., Franceschi, J., Parlow, E., Adler, B., Kalthoff, N., Cermak, J., Andersen, H., Fuchs, J., Bott, A., Hacker, M., Wagner, N., Maggs-Kölling, G., Wassenaar, T. and Seely, M.: Probing the fog life-cycles in the Namib desert, Bull. Am. Met. Soc., 100, 2491-2508, doi:10.1175/bams-d-18-0142.1, 2019.

Swan, H.B., and J. P. Ivey, Elevated particulate methanesulfonate, oxalate and iron over Sydney Harbour in the austral summer of 2019-20 during unprecedent bushfire activity, Atmos. Environ., 226, 118739, https://doi.org/10.1016/j.atmosenv.2021.118739, 2021.

Swap, R., Garstang, M., Macko, S.A., et al., The long–range transport of southern African aerosols to the tropical South Atlantic. J. Geophys. Res., 101, 23777–23791, https://doi.org/10.1029/95jd01049, 1996.

Takahashi, Y., Higashi, M., Fukurawa, T., Mitsunobu, S.: Change of iron species and iron solubility in Asian dust during the long-range transport from western China to Japan, Atmos. Chem. Phys, 11, 11237-11252, doi:10.5194/acp-11-11237-2011, 2011.

Tao, Y., Murphy, J.G.: The mechanisms responsible for the interactions among oxalate, pH, and Fe dissolution in $PM_{2.5}$. Earth and Space Chemistry, 3, 2259-2265, https://doi.org/10.1021/acsearthspacechem.9b00172, 2019.

Tegen, I., Schepanski, K.: The Global distribution of Mineral Dust, IOP Conference Series: Earth and Environmental Sciences, 7, 012001, doi:10.1088/1755-1307/7/1/012001, 2009.

Tyson, P. D. and Preston-Whyte, R. A.: The Weather and Climate of Southern Africa, 2nd ed., Oxford University Press Southern Africa, Cape Town, 2014.

Ventura, A., Simões, E.F.C., Almeida, A.S., Martins, R., Duarte, A.C., Loureiro, S., Duarte, R.M.B.O., Deposition of aerosols onto upper ocean and their impacts on marine biota, Atmosphere, 12, 684, https://doi.org/10.3390/atmos12060684, 2021.

Vickery, K.J., Eckardt, F.D.: Dust emission controls on the lower Kuiseb River valley, Central Namib, Aeolian Res., 10, 125-133, https://doi.org/10.1016/j.aeolia.2013.02.006, 2013.

von Holdt, J.R., Eckardt, F.D., Wiggs, G.F.S.: Landsat identifies aeolian dust emission dynamics at the landform scale, Remote Sensing Environ., 198, 229-243, https://doi.org/10.1016/j.rse.2017.06.010, 2017.

Wozniak, A. S.; Shelley, R. U.; Sleighter, R. L.; Abdulla, H. A. N.; Morton, P. L.; Landing, W. M.; Hatcher, P. G. Relationships among aerosol water soluble organic matter, iron and aluminium in European, North African,

and Marine air masses from the 2010 US GEOTRACES cruise, Mar. Chem., 154, 24– 33 DOI: 10.1016/j.marchem.2013.04.011, 2013.

Wozniak, A. S., R.U. Shelley, S.D. McElhenie, W.M. Landing, P. G. Hatcher. Aerosol water soluble organic matter characteristics over the North Atlantic Ocean: Implications for iron-binding ligands and iron solubility. SCOR WG 139: Organic Ligands – A Key Control on Trace Metal Biogeochemistry in the Ocean 173: 162-72. https://doi.org/10.1016/j.marchem.2014.11.002, 2015.

Zhuang, G., Z. Yi, R. A. Duce, and Brown, P.R.: Link between iron and sulphur cycles suggested by detection of Fe (II) in remote marine aerosols, Nature, 355, pp. 537–539, https://doi.org/10.1038/355537a0, 1992.